Multiplexing Scheme for Initial Access Control Signals Using Dedicated Frequency Bandwidth in Sub-THz Communications

Mamoru Sawahashi
Tokyo City University
Tokyo, Japan

Takashi Ohiwa
Tokyo City University
Tokyo, Japan

Satoshi Suyama
NTT DOCOMO INC.
Kanagawa, Japan

***Abstract*—This paper proposes a scheme that multiplexes control signals for initial access using a dedicated frequency bandwidth in the sub-Terahertz (THz) bands. We employ subcarrier spacings (SCSs) in a dedicated frequency bandwidth that are narrower than those for other frequency bandwidths that multiplex shared channels used to convey user data and control channels in the physical layer in both the downlink (DL) and uplink (UL). The estimation accuracy of fractional frequency offset (FFO) based on the autocorrelation using the cyclic prefix (CP) that is attached to each discrete Fourier transform-spread orthogonal frequency division multiplexing (DFT-S-OFDM) symbol is improved due to the increase in the CP power as the SCS becomes narrower. Accordingly, the narrower SCSs for the control signals in the initial access enable us to achieve a high physical layer cell ID detection probability by making effective use of the FFO estimation and joint estimation of the integer frequency offset (IFO) and primary synchronization signal (PSS) in the DL. Moreover, the narrow SCS achieves a relaxed round trip time delay measurement based on the physical random access channel (PRACH) with a low computational complexity in the UL. We also present a synchronization signal block structure in the DL and PRACH structure in the UL that are suitable for the sub-THz bands.**

***Index Terms*—initial access, sub-THz bands, synchronization signal block, PRACH, carrier frequency offset**

I. Introduction

In 3rd Generation Partnership Project (3GPP), enhanced mobile broadband (eMBB), massive machine type communications (mMTC), and ultra reliable low latency communications (URLLC) are the main use cases specified in the 5G New Radio (NR) interface [1], [2]. In wireless communications, the amount of Information-of-Things (IoT) traffic that is generated by mMTC or URLLC is larger than that for eMBB [3]. It is anticipated that the amount IoT traffic will further increase significantly due to industrial IoT including factory IoT and vehicular-to-everything (V2X). It is stipulated that the 3GPP NR radio interface employing the orthogonal frequency division multiplexing (OFDM) waveform is used in frequency spectra up to 71 GHz [4]. In addition, a wide subcarrier spacing (SCS) up to 960 kHz was adopted in the NR specifications [4]. Recently, frequency spectra in the sub-Terahertz (THz) range such as 100 GHz - 300 GHz have drawn attention as a promising candidate for the beyond 5G systems [5] - [7].

Discrete Fourier transform (DFT)-spread OFDM (DFT-S-OFDM) [8], [9] was adopted in the LTE uplink (UL) and the NR UL with single-stream transmission because it achieves a lower peak-to-average power ratio (PAPR) than OFDM. In NR, different SCSs are adopted and the length of the cyclic prefix (CP) appended to each OFDM symbol is different according to the SCS. Zero-tail DFT-S-OFDM was then proposed to accommodate multiple numerologies using different CP lengths according to the propagation delay [10]. Moreover, a generalized DFT-S-OFDM was proposed for supporting diverse services by employing the zero-tail DFT-S-OFDM [11]. Variations of the DFT-S-OFDM waveform using a zero internal guard interval, unique word, and pulse shaping were investigated and analyzed in [12]. Beamforming transmission and reception are necessary to extend the coverage area for a large propagation loss in the millimeter-wave (mmW) bands [1], [2]. In the sub-THz bands, a high-power-efficient waveform with a low PAPR is necessary in addition to the mandatory use of beamforming transmission and reception. Therefore, DFT-S-OFDM is a promising waveform candidate in the sub-THz bands beyond 71 GHz [5] - [7].

This paper focuses on the initial access control signals in the physical layer for the sub-THz bands. In the NR specifications, a synchronization signal block (SSB) or an SS/physical broadcast channel (PBCH) block is stipulated that includes signals required for the downlink (DL) initial access for a set of user equipment (UE) during intermittent reception [1]. The SSB consists of a primary synchronization signal (PSS), secondary synchronization signal (SSS), and PBCH [1]. In the DL initial access, a UE first searches for the physical layer cell ID (PCID) of the target cell that provides the highest received power level to the UE of interest from the detected PSS and SSS sequences. After that, the UE decodes the master information block (MIB) that is multiplexed in the PBCH payload. The MIB contains control signals including resource information of system information block 1 (SIB1), which is carried by the succeeding physical downlink shared channel (PDSCH) [2]. After establishing a radio link in the DL, a UE transmits the physical random access channel (PRACH) first in the UL. The PRACH comprises a CP and preamble sequence with repeated transmission in the NR specifications [1], [2]. In some PRACH formats, a guard period is added. A PRACH in the UL initial access is a contention channel because multiple UEs transmit a PRACH in the same physical

resource block (PRB) in the frequency and time domains. In beyond 5G systems in the sub-THz bands, designs of control signals for initial access including the SSB in the DL and the PRACH and relevant physical channels in the UL are crucial for establishing access links quickly and accurately. Note that although we assume the waveform of DFT-S-OFDM in this paper, the control signal structures for initial access can be applied to OFDM due to high commonality.

This paper proposes a scheme that multiplexes control signals for initial access using a dedicated frequency bandwidth in the sub-THz bands. The main point of the proposed scheme is to multiplex control signals for initial access in the dedicated frequency bandwidth with SCSs that are narrower than those for other frequency bandwidths that multiplex shared channels conveying user data and control channels in the physical layer for both the DL and UL. By employing the narrow SCSs for SSB in the DL, we achieve a high PCID detection probability in the low received signal-to-noise (SNR) region, which corresponds to the condition of a UE located at a cell edge. Moreover, the narrow SCS achieves a relaxed round trip time delay (RTD) measurement based on the PRACH with a low computational complexity in the UL. This paper is a semi-tutorial paper in the sense that the proposed methods are based on the results of state-of-the-art literature and our previous papers. The reminder of the paper is organized as follows. In Section II, we describe the proposed control-signal multiplexing scheme for initial access employing a dedicated frequency bandwidth with out-band and in-band resources in the sub-THz bands. Next, in Section III, we describe the SSB structure and the PCID detection method using synchronization signals. Subsequently, in Section IV, we discuss the PRACH structure and RTD when using the proposed multiplexing scheme in a dedicated frequency bandwidth in the sub-THz bands. Finally, Section V gives our concluding statements.

II. Resource Bandwidth Dedicated to Control Signals for Initial Access

In the sub-THz bands, a much wider frequency spectrum such as a bandwidth of a few gigahertz is available. It is anticipated that the system bandwidth of a base station (BS) and the channel bandwidth of a UE transmission will be wider than those in the 5G NR specifications. Hence, the application of an even wider SCS was proposed for beyond 5G systems employing the sub-THz bands [13]. Meanwhile, propagation path loss due chiefly to distance-dependent path loss increases significantly in the sub-THz bands. Based on the link budget in [7], the maximum line-of-sight (LOS) distance for providing 100 Gbps is below 20 m with the total equivalent isotropic radiation power of 48.8 dBm in a 20-GHz bandwidth at the carrier frequency of 120 GHz. Meanwhile, the requirement of the PCID detection probability and that for the PBCH block error rate should be satisfied at a UE receiver in the DL. Similarly, the required miss detection probability (MDP) of the PRACH should be achieved at a BS receiver in the UL for all UEs located within a cell. Therefore, in addition to the essential use of beamforming transmission and reception, the narrower transmission bandwidth than that for the shared channels carrying user data and the related control channels is effective in extending the coverage distance for the SSB, PRACH, and associated physical channels in the sub-THz bands.

In this paper, we propose two frequency bandwidth assignment schemes for the initial-access control signals: out-band and in-band frequency bandwidth assignment schemes.

• Out-band frequency bandwidth assignment scheme for initial access signaling

In the out-band frequency bandwidth assignment for initial-access control signals, we use physical channels that are required for the initial access of the NR radio interface in the sub-6-GHz bands or mmW bands. After establishing initial access, a UE receives and transmits high-layer control signals and user data using shared channels and control channels in the sub-THz bands. Since the DFT-S-OFDM symbol duration is very short due to the wide SCS, a high bit rate of greater than 1 Gbps and very low latency are achieved in the sub-THz bands.

• In-band frequency bandwidth assignment scheme for initial access signaling

Fig. 1 shows the proposed frequency bandwidth assignment scheme of the control signals for initial access in the sub-THz bands. In the proposed scheme, we multiplex control signals for initial access in the dedicated frequency bandwidth. In the dedicated frequency bandwidth that comprises one or multiple PRBs, SCSs are employed that are narrower than those for the other frequency bandwidths for multiplexing shared channels and the associated physical layer control channels. For instance, the dedicated frequency bandwidth employs a 120-kHz SCS, while the SCS of 1 MHz to a few megahertz is used for the shared channels that convey user data and the associated control channels in the sub-THz bands. In the dedicated frequency bandwidth, we multiplex an SSB in the DL, and multiplex the PRACH and related physical channels in the UL assuming TDD. Because we use a narrow SCS, we can design a long DFT-S-OFDM symbol length associated with a long CP length that is at the same level as that in the case of a 120-kHz SCS in the NR specifications. We also maintain the same PRACH preamble length as that in the NR specifications. In addition, we can multiplex high-layer control signals in the dedicated bandwidth. Similar to the LTE and NR specifications, the center frequency of the SSB in the dedicated frequency bandwidth is located on the frequency raster that is to be specified in the sub-THz bands.

Meanwhile, the physical downlink control channel (PDCCH) and physical uplink control channel (PUCCH) are multiplexed in the resource bandwidth employing wide SCSs, in which PDSCH and physical uplink shared channel (PUSCH) are multiplexed. Because wide SCSs are employed in the frequency bandwidths, the DFT-S-OFDM symbol length and the resultant slot length become very short. Hence, ultra-high data rate transmission is possible and a very short transmission delay, *i.e.,* latency such as 0.1 ms, is achieved even including the delay due to hybrid automatic repeat request (HARQ).

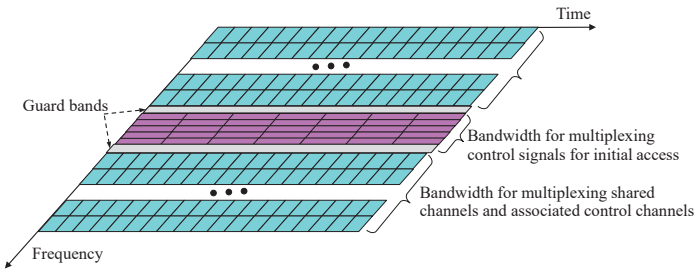

Fig. 1. Proposed resource assignment of control signals in the frequency domain for initial access.

III. SSB Structure and PCID Detection Method

A. Hardware Impairments in Sub-THz Bands

The hierarchical synchronization signal configuration comprising the PSS and SSS is adopted in the LTE and NR specifications to reduce the computational complexity for PCID detection. It is natural that the hierarchical SS configuration is used in the beyond 5G systems in the sub-THz bands. Facing the increasing number of cells, particularly small cells with high traffic density, it is desirable to increase the number of PCIDs, N_{ID}^{cell}, to 2,016, *e.g.*, twice that in the NR specifications. The PCID, N_{ID}^{cell}, is represented as [1]

$$N_{ID}^{cell} = 3N_{ID}^{(1)} + N_{ID}^{(2)}. \tag{1}$$

In (1), $N_{ID}^{(1)}$ indicates the PCID group index ($N_{ID}^{(1)} \in \{0, 1, \ldots, 671\}$) and $N_{ID}^{(2)}$ indicates the PCID index within the same PCID group ($N_{ID}^{(2)} \in \{0, 1, 2\}$) assuming the identical hierarchical PCID configuration as in the NR specifications. The PSS sequence represents $N_{ID}^{(2)}$ while the SSS sequence represents $N_{ID}^{(1)}$. The number of $N_{ID}^{(1)}$ will be increased when the number of PCIDs increases. Consequently, the sequence length of the PSS and SSS will be longer than 127, which is the specified length in the NR specifications. In the mmW bands, major impairments that degrade the initial PCID detection probability are an increasing carrier frequency offset (CFO) and phase noise (PN). The CFO is caused by the frequency stability of a UE local oscillator that is worse by two orders of magnitude than that for a BS local oscillator. The PN is induced in the BS and UE local oscillators.

1) CFO: For establishing a radio link in the initial access, a UE first searches for an SSB that is transmitted periodically. A UE detects the received timing and the sequences of the PSS and SSS in the SSB with the free-running frequency stability of its local oscillator, *i.e.*, in the order of a few parts per million (ppm). Hence, the CFO due to the degraded frequency stability of the free-running local oscillator of a UE is the most significant hardware impairment to the PCID detection. The CFO, Δf, is represented as $\Delta f = \varepsilon \times f_c$. Thus, the CFO becomes larger according to the increase in the f_c value. For a large f_c or ε value, the phase rotation caused by the CFO in the interval between the PSS and SSS exceeds 2π, *i.e.*, $\pm\pi$. In such a case, the CFO, Δf, is represented as $\Delta f = \Delta f_{FFO} + \Delta f_{IFO}$. Here, Δf_{FFO} denotes a fractional frequency offset (FFO) that provides the phase rotation in the range from -π to +π in measurement interval T_{Int}. Term Δf_{IFO} indicates an integer frequency offset (IFO) that provides the phase rotation of $2\pi G$, where $|G|$ is an integer of 1 or greater.

2) PN: PN in the mmW bands is modeled by a discrete-time Wiener process as $\theta_n = \theta_{n-1} + \Delta_n$ [14]. Here, θ_n denotes PN at sample timing n and Δ_n denotes a zero mean Gaussian increment, $\Delta_n \sim \mathcal{N}(0, \sigma_\Delta^2)$ (variance σ_Δ^2 denotes PN). A discrete time PN signal in the time domain is generated by passing white Gaussian noise through an infinite impulse response (IIR) or finite impulse response (FIR) low-pass filter [15], [16]. Because transmission bandwidths will become much wider than that in the mmW bands, it is reported in [17] - [19] that the effect of the PN in the sub-THz bands will become larger than that in the mmW bands. It is also reported in [18] and [17] that the PN in the sub-THz bands comprises the correlated Wiener PN and uncorrelated Gaussian PN that appear in a high frequency region away from the center of the transmission bandwidth. Hence, [18] proposed a PN model for the sub-THz bands that superposes the correlated Wiener PN with the attenuation of 20 dB per decade and the uncorrelated Gaussian PN.

B. Proposed SSB Structure

Fig. 2(a) shows the SSB structure in the NR specifications [1]. In the NR specifications, the SSB configuration was investigated and specified by the 3GPP in [20]. Let T_{OFDM} be the OFDM or DFT-S-OFDM symbol duration, then measurement interval T_{Int} is given as $T_{Int} = M \times T_{OFDM}$ when the distance between the PSS and SSS is M OFDM symbol duration. The maximum FFO range is given in the next equation.

$$\Delta f_{FFO} = \pm\frac{1}{2T_{Int}} = \pm\frac{1}{2M} f_{SCS} \tag{2}$$

In (2), f_{SCS} denotes an SCS. Hence, according to an increase in the M figure, the measurable frequency range for FFO becomes narrow. In the NR radio interface, the SSB structure is decided in which the distance between the PSS and SSS is one OFDM symbol duration [20]. In the sub-THz bands, IFO estimation is necessary in addition to the FFO estimation because the phase rotation due to the CFO in the interval between the PSS and SSS exceeds 2π. Hence, we propose the SSB structure shown in Fig. 2(b). The proposed SSB structure has two features. First, the transmission bandwidth of the PSS and SSS is the same as that for the PBCH. Second, the PBCH is multiplexed in the OFDM symbol positions between the PSS and SSS. The major aim of the proposed SSB structure is to eliminate the demodulation reference signal (DMRS) in the PBCH. By multiplexing the PBCH between the PSS and SSS, accurate channel estimation for PBCH symbols is possible leveraging the PSS and SSS. Table I gives a comparison of the features of the SSB structure for the NR interface and that for the proposed SSB structure. The effect of the CFO becomes larger in accordance with the increase in the applied frequency spectrum in the sub-THz bands. Hence, the application of cyclic-shifted M sequences is suitable as the PSS and SSS sequences because the M-sequence is more robust for a large

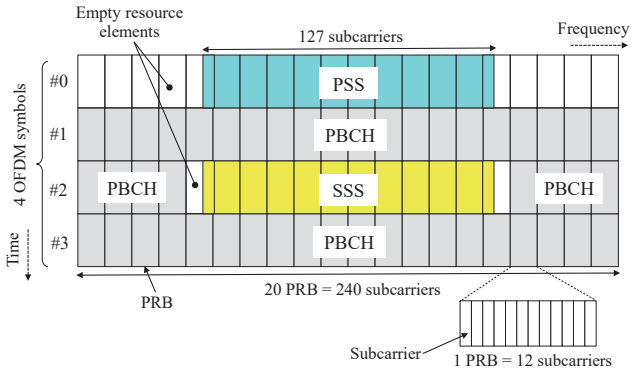

(a) SSB structure in NR specifications

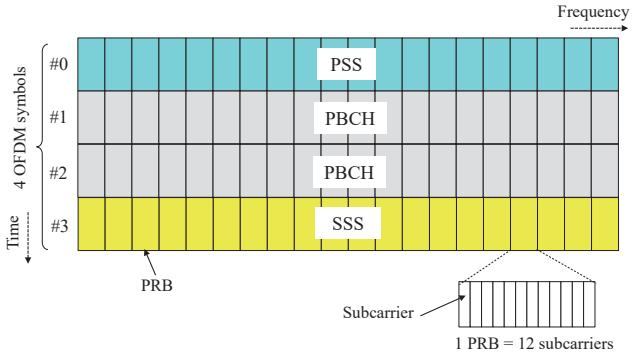

(b) Proposed SSB structure

Fig. 2. SSB structure for DL initial access.

TABLE I
MULTIPLEXING SCHEME IN SSB

	Same transmission bandwidth	Different transmission bandwidths between PSS & SSS and PBCH (NR)
DMRS in PBCH	Unnecessary	Necessary in PBCH resource elements (REs) outside of PSS & SSS
Power boosting of PSS	Necessary to decrease transmission power of other symbols in same DFT-S-OFDM symbol	Flexible power boosting due to empty REs

CFO than the Zadoff-Chu sequence [21], which was proven in the NR specifications.

C. PCID Detection Method

There are two major methods for PCID detection for the best cell including the FFO and IFO compensation in the DFT-S-OFDM or OFDM waveform. The first method is an FFO estimation based on the partial correlation of the PSS and joint detection of the IFO and SSS sequence [22], [23]. The second method is an FFO estimation based on the autocorrelation using a CP and the joint estimation of the IFO and PSS [24], [25]. Members of our research group showed that the PCID detection method with the FFO estimation based on autocorrelation using a CP and joint estimation of the IFO and PSS achieves a higher PCID detection probability than that with the FFO estimation based on the PSS correlation and joint detection of the IFO and SSS sequence in the presence of a large CFO in the mmW bands [26]. So, here we briefly explain the PCID detection method with the FFO estimation based on autocorrelation using a CP and the joint estimation of the IFO and PSS. Fig. 3 shows the flow for the PCID detection method. The received SS burst set signal in DL that suffers from multipath fading in the tapped delay line channel model is given as $r^{(\eta)}(n) = \sum_{\nu=1}^{N} h_{\nu}^{(\eta)} D(n-\tau_{\nu}) e^{j2\pi n \Delta f/f_s} e^{j\theta_n} + w^{(\eta)}(n)$. Here, n is a sample index, ν is a tap index, and N denotes the number of multipaths. Moreover, $f_s = 1/T_s$ indicates the sampling frequency, where T_s is the sample duration. Term $D(n)$ represents transmitted signals including the SS burst set, Δf is the CFO, θ_n is PN, and $w^{(\eta)}(n)$ is additive white Gaussian noise with zero mean. We first detect the tentative DFT-S-OFDM symbol timing at which the maximum autocorrelation power using the CP is provided as shown in the next equation [24], [25].

$$\begin{aligned}\hat{\tau} \;=\; & \arg\max_{\tau} \sum_{\eta=0}^{N_{Rx}-1} \sum_{\lambda=0}^{\Lambda-1} \sum_{n=0}^{N_{CP}-1} \Big\{ r^{(\eta)}\big(\tau+n \\ & +\lambda(N_{CP}+N_{FFT})\big)^{*} \cdot r^{(\eta)}\big(\tau+n+N_{FFT} \\ & +\lambda(N_{CP}+N_{FFT})\big) \Big\} \end{aligned} \tag{3}$$

In (3), N_{CP} is the number of samples in the CP length and N_{FFT} is the number of samples in the DFT-S-OFDM symbol length. Moreover, Λ denotes the number of averaging correlations using the CP and $*$ denotes a complex conjugate. Next, we estimate the FFO as [24], [25]

$$\begin{aligned}\Delta\hat{f}_{FFO} \;=\; & \frac{f_s}{2\pi N_{FFT}} \arg \sum_{\eta=0}^{N_{Rx}-1} \sum_{\lambda=0}^{\Lambda-1} \sum_{n=0}^{N_{CP}-1} \\ & \Big\{ r^{(\eta)}\big(\hat{\tau}+n+\lambda(N_{CP}+N_{FFT})\big)^{*} \cdot r^{(\eta)}\big(\hat{\tau}+n \\ & +N_{FFT}+\lambda(N_{CP}+N_{FFT})\big) \Big\}. \end{aligned} \tag{4}$$

When we let $\tilde{r}(n)$ be the received signal after compensating for the FFO, it is given as $\tilde{r}(n) = r(n)e^{-2\pi n \Delta\hat{f}_{FFO}/f_s}$. The IFO, Δf_{IFO}, is represented as $\Delta f_{IFO} = \frac{G f_s}{M \times N_{FFT}}$. We jointly estimate the received timing and sequence of the PSS, and the G value of the IFO, with which the maximum cross-correlation power between the signal $\tilde{r}(n)$ and the PSS sequence candidates is provided as shown in the next equation [25].

$$\begin{aligned}(\hat{\tau}, \hat{N}_{ID}^{(2)}, \hat{G}) \;=\; & \arg\max_{\tau, N_{ID}^{(2)}, G} \sum_{\eta=0}^{N_{Rx}-1} \Bigg| \sum_{\upsilon=0}^{N_{FFT}-1} \tilde{r}^{(\eta)}\big(\tau+\upsilon\big) \\ & \cdot e^{-j2\pi G \frac{\upsilon}{N_{FFT}}} \cdot \bar{d}_{PSS}\,(\upsilon)^{*} \Bigg|^{2} \end{aligned} \tag{5}$$

In (5), $\bar{d}_{PSS}(n)$ denotes the PSS sequence in the time domain that is given as $\bar{d}_{PSS}(n) = \frac{1}{\sqrt{N_{FFT}}} \sum_{\upsilon=0}^{N_{FFT}-1} D_{PSS}(\upsilon) \exp\left(\frac{j2\pi n\upsilon}{N_{FFT}}\right)$. We compensate for the CFO of the received signal using the estimated FFO, $\Delta\hat{f}_{FFO}$, and the $\hat{G}$ value of the IFO, as $\tilde{r}_n = r_n \exp\big(-2\pi n \frac{(\Delta\hat{f}_{FFO} + \hat{G} f_s/N_{FFT})}{f_s}\big)$. By using the FFT, the PSS and SSS in time domain are converted into frequency domain signals to $\tilde{R}_{PSS/SSS}^{(\eta)}(k) =$

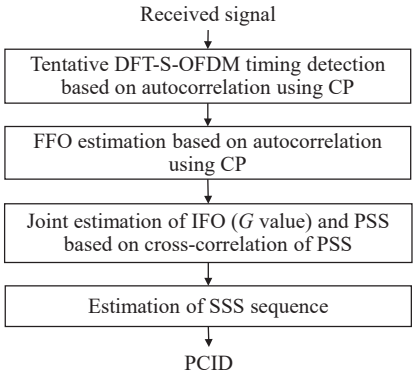

Fig. 3. Flow of PCID detection method with FFO estimation based on autocorrelation using CP and joint estimation of IFO and PSS.

$\sum_{n=0}^{N_{FFT}-1} \tilde{r}^{(\eta)}_{PSS/SSS}(n) \exp(-j2\pi nk/N_{FFT})$. We multiply the complex conjugate of the estimated channel gain at subcarrier k, $\bar{H}^{(\eta)}(k)$, and that of the SSS sequence replica, $d_{SSS}(k)^*$, to the received SSS. We detect the SSS sequence that provides the maximum correlation power level as shown in the equation below [23].

$$\hat{N}^{(1)}_{ID} = \arg\max_{N^{(1)}_{ID}} \left| \sum_{\eta=0}^{1} \sum_{k=0}^{126} \tilde{R}^{(\eta)}_{SSS}(k) \cdot \bar{H}^{(\eta)}(k)^* \cdot d_{SSS}(k)^* \right|^2 \quad (6)$$

We identify the PCID from the detected PSS and SSS sequences. In the aforementioned PCID detection method, the CFO in the SSS from the PSS received timing is estimated and compensated. When the CFO is extremely large, the detection error of the PSS received timing occurs due to the relative time shift between the received signal and the PSS replica over the PSS sequence length. In such a case, computation of the correlation of the PSS in the frequency domain is necessary at the sacrifice of increasing the computational complexity [27]. In terms of the PN, we showed that the effect of the Wiener PN on the PCID detection probability is not large in the mmW bands. Meanwhile, the uncorrelated Gaussian PN of the PN in the sub-THz bands degrades the required received SNR satisfying the target PCID detection probability [28].

IV. PRACH Structure

New PRACH formats using a short sequence are specified in addition to the PRACH formats with a long sequence in the NR specifications [1], [2], [29]. As a PRACH preamble sequence, a Zadoff-Chu sequence is adopted [1]. The cross-correlation between different cyclic shifts (CSs) with the same root index (RI) is zero for the Zadoff-Chu sequence. Hence, for multiplexing multiple PRACH preambles from different UEs asynchronously, CS multiplexing is used with higher priority than the multiplexing method employing different RIs. The CFO due to the frequency error of a UE local oscillator affects the PRACH detection probability since the received timing of the Zadoff-Chu sequence is shifted according to the applied CS value [30]. Meanwhile, at the timing when a UE transmits the PRACH, the UE has already detected the PCID and decoded the MIB in the PBCH payload, and the SIB 1 bits that are carried by the PDSCH in the DL. As a result, the frequency error of a UE local oscillator is reduced to approximately 1/10 of the free-running frequency by measuring the more accurate frequency of a BS through DL physical channels. A UE transmits the PRACH after pre-compensating the CFO. Consequently, the residual CFO in the PRACH is suppressed to a low level. Members of our research group proposed the PRACH transmission method employing pre-compensation of the CFO that is estimated using the SSB at a UE in [31]. It was shown that a PRACH MDP that is almost identical to that without CFO is achieved when the average received SNR at a UE is higher than approximately -5 dB for the frequency stability of a UE local oscillator of up to 3 ppm [31].

Therefore, the remaining major impairment is PN caused by local oscillators. In the sub-THz bands, use of a much wider SCS for the PRACH was proposed for mitigating the effect of PN [13]. At a BS receiver, multiple PRACHs are received simultaneously and asynchronously at the same frequency and time resource due to the different RTDs according to the UE location. A BS measures the RTD of each UE based on the received timing of the PRACH. In the NR specifications, the CP length is designed so that it becomes longer than the RTD for the supported cell distance. However, according to the increase in the SCS, the CP length and OFDM or DFT-S-OFDM symbol length becomes shorter than the RTD. Hence [13] proposed a PRACH structure and two-step RTD measurement method for when the RTD is much longer than the DFT-S-OFDM symbol length for a wide SCS in the sub-THz bands.

In the proposed PRACH transmission method leveraging the dedicated resource in the frequency domain to control signals for initial access, the SCS is for instance 120 kHz or 480 kHz at most. We let T_{OFDM} be the length of the effective DFT-S-OFDM symbol that is represented as $T_{OFDM} = 1/f_{SCS}$. The maximum distance between a BS and a UE from the viewpoint of the RTD is given as $d_{cell} = \frac{1}{2}c{\cdot}T_{OFDM}$ [29]. When the SCS is 120 kHz and 480 kHz, d_{cell} becomes 1,250 m and 312.5 m, respectively. Hence, by employing a relatively narrow SCS compared to those for data channels and associated control channels, a sufficient cell distance is achieved in the sub-THz bands.

However, when supporting wide coverage, the RTD becomes larger than the d_{cell} value. In such a case, the two-step RTD measurement method that was proposed in [13] is beneficial. In this case, a PRACH sequence that comprises different Zadoff-Chu sequences is necessary. Some PRACH sequences that concatenate different Zadoff-Chu sequences were proposed for estimating the large CFO and Doppler shifts in non-terrestrial networks employing satellites [32] - [34]. A similar PRACH structure was proposed in [13], in which a guard period is inserted between the first and second PRACH sequences. Fig. 4 shows an example of the PRACH structure. The first PRACH sequences is repeated to extend the achievable distance, *i.e.*, coverage area. Fractional timing in the RTD is measured based on the correlation of the first PRACH sequence. Integer timing that represents integer times of the PRACH sequence length that corresponds to one

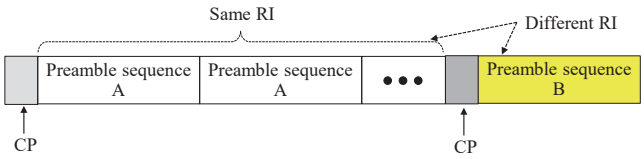

Fig. 4. Example of PRACH structure.

DFT-S-OFDM symbol duration is estimated by employing the correlation of the second PRACH sequence. We assign different RIs to the first and second PRACH sequences. By assigning different cyclic shift resources to the different PRACH sequences, the mutual cross-correlation among the simultaneously accessing PRACHs is reduced to a low a level as possible [2].

V. Conclusion

This paper proposed a multiplexing scheme for initial-access control signals employing a dedicated frequency bandwidth for sub-THz communications. We employ SCSs in a dedicated frequency bandwidth that are narrower than those used for other frequency bandwidths in which user data are conveyed using the DL and UL shared channels and the associated control channels in the physical layer in the sub-THz bands. By employing a narrow SCS for the SSB in the DL, we achieve a high PCID detection probability in a low received SNR region, which corresponds to the condition of a UE located at a cell edge. Moreover, a narrow SCS achieves a relaxed RTD measurement based on the PRACH with a low computational complexity in the UL. We also presented an SSB structure for reducing the RS overhead in the DL and the PRACH structure for relaxed RTD measurement in the UL that are applicable in the sub-THz bands.

Acknowledgment

This research and development work was supported by MIC/SCOPE JP225003003.

References

[1] 3GPP TS 38.211 "NR; Physical channels and modulation (Release 15)," V15.6.0 , June 2019.
[2] C. Johnson, 5G New Radio in Bullets, 2019.
[3] Cisco Annual Internet Report (2018–2023) White Paper.
[4] 3GPP TR 38.808, "Study on supporting NR from 52.6 GHz to 71 GHz," V17.0.0, March 2021.
[5] J.-B. Dore, Y. Corre, S. Bicais, J. Palicot, E. Faussurier, D. Ktenas, and F. Bader, "Above-90GHz spectrum and single-carrier waveform as enablers for efficient Tbit/s wireless communications," Proc. 2018 25th International Conference on Telecommunications (ICT), June 2018.
[6] O. Tervo, T. Levanen, K. Pajukoski, J. Hulkkonen, P. Wainio, and M. Valkama, "5G New radio evolution towards sub-THz communications," Proc. 2020 2nd 6G Wireless Summit (6G SUMMIT), March 2020.
[7] H. Halbauer and T. Wild, "Towards power efficient 6G sub-THz transmission," Proc. 2021 Joint European Conference on Networks and Communications & 6G Summit (EuCNC/6G Summit), June 2021.
[8] D. Galda and H. Rohling, "A low complexity transmitter structure for OFDM-FDMA uplink system," Proc. IEEE VTC2002-Spring, vol. 4, pp. 1737-1741, May 2002.
[9] R. Dinis, D. Falconer, C. T. Lam, and M. Sabbaghian, "A multiple access scheme for the uplink of broadband wireless access," Proc. IEEE GLOBECOM'2004, vol. 6, pp. 3808-3812, Dec. 2004.
[10] G. Berardinelli, F. M. L. Tavares, T. B. Sorensen, P. Mogensen, and K. Pajukoski, "Zero-tail DFT-spread-OFDM signals," Proc. 2013 IEEE Globecom Workshops (GC Wkshps), Dec. 2013.
[11] G. Berardinelli, K. I. Pedersen, T. B. Sorensen, and P. Mogensen, "Generalized DFT-spread-OFDM as 5G waveform," IEEE Commun. Mag., vol. 54, no. 11, pp. 99 - 105, Nov. 2016.
[12] A. Sahin, R. Yang, E. Bala, M. C. Beluri, and R. L. Olesen, "Flexible DFT-S-OFDM: Solutions and challenges," IEEE Commun. Mag., vol. 54, no. 11, pp. 106 - 112, Nov. 2016.
[13] S. Lee, W. Jeong, J. Jung, J. Lee, and S. Choi, "A new preamble signal design for random access in sub-Terahertz 6G cellular systems," Proc. 2022 IEEE International Conference on Communications Workshops (ICC Workshops), May 2022.
[14] N. J. Kasdin, "Discrete simulation of colored noise and stochastic processes and $1/f^{\alpha}$ power law noise generation," Proceedings of the IEEE, vol. 83, no. 5, pp. 802 - 827, May 1995.
[15] C.-S. Choi, Y. Shoji, H. Harada, R. Funada, S. Kato, K. Maruhashi, I. Toyoda, and K. Takahashi, "RF impairment models for 60GHz-band SYS/PHY simulation," IEEE document 802.15-06-0477-01-003c, Nov. 2006.
[16] N. Kamiya and E. Sasaki, "Pilot-symbol assisted and code-aided phase error estimation for high-order QAM transmission," IEEE Trans. on Commun., vol. 61, no. 10, pp. 4369-4380, Oct. 2013.
[17] S. Bicais and J.-B. Dore, "Phase noise model selection for sub-THz communications," Proc. IEEE Globecom 2019, Dec. 2019.
[18] P. Neshaastegaran and M. Jian, "On the effect of oscillator phase noise on the performance of OFDM systems in sub-THz band," Proc. ICSPCS 2020, Dec. 2020.
[19] M. Sarajlic *et al.*, "Waveforms for sub-THz 6G: Design guidelines," Proc. 2023 Joint European Conference on Networks and Communications & 6G Summit (EuCNC/6G Summit), June 2023.
[20] Z. Lin, J. Li, Y. Zheng, N. V. Irukulapati, H. Wang, and H. Sahlin, "SS/PBCH block design in 5G New Radio (NR)," Proc. 2018 IEEE Globecom Workshops (GC Wkshps), Dec. 2018.
[21] D. C. Chu, "Polyphase codes with good periodic correlation properties," IEEE Trans. Inform. Theory, vol. 18, pp. 531-532, July 1972.
[22] S. Nagata, Y. Kishiyama, M. Tanno, K. Higuchi, and M. Sawahashi, "Cell search time comparison using hierarchical and non-hierarchical synchronization channels in OFDM based evolved UTRA downlink," in Proc. IEEE VTC2007-Spring, May 2007.
[23] D. Inoue, K. Ota, M. Sawahashi, and S. Nagata, "Physical cell ID detection using joint estimation of frequency offset and SSS sequence for NR initial access," IEICE Trans. on Commun., vol. E104-B, no. 9, pp. 1120 - 1128, Sept. 2021.
[24] Q. Wang, C. Mehlführer, and M. Rupp, "Carrier frequency synchronization in the downlink of 3GPP LTE," Proc IEEE PIMRC2010, Sept. 2010.
[25] 3GPP TSG RAN WG1, R1-1702822, "Discussion and evaluation on NR-PSS/SSS structure," NTT DOCOMO INC. Feb. 2017.
[26] S. Yoneda, M. Sawahashi, and S. Nagata, "Comparisons of physical cell ID detection methods with carrier frequency offset compensation for millimeter-wave bands," in Proc. IEEE VTC2022-Fall, Oct. 2022.
[27] D. Wang, Z. Mei, H. Zhang, H. Li, "A novel PSS timing synchronization algorithm for cell search in 5G NR system," IEEE Access, vol. 9, pp. 5870 - 5880, Jan. 2021.
[28] T. Ohiwa, Y. Mabuchi, M. Sawahashi, S. Nagata, and S. Suyama, "PCID detection probabilities in the presence of CFO and strong phase noise in sub-THz bands," in Proc. APCC2024, Nov. 2024.
[29] A. Chakrapani, "On the design details of SS/PBCH, signal generation and PRACH in 5G-NR," IEEE Access, vol. 8, pp. 136617 - 136637, July 2020.
[30] M. Hua, M. Wang, W. Yang, X. You, F. Shu, J. Wang, W. Sheng, and Q. Chen, "Analysis of the frequency offset effect on random access signals," IEEE Trans. on Commun., vol. 61, no. 11, pp. 4728 - 4740, Nov. 2013.
[31] S. Yoneda, M. Sawahashi, and S. Nagata, "Detection probability of PRACH employing carrier frequency offset compensation at UE transmission in NR uplink," Proc. 2023 International Conference on Wireless Communications and Signal Processing (WCSP), Nov. 2023.
[32] L. Zhen, H. Qin, B. Song, R. Ding, X. Du, and M. Guizani, "Random access preamble design and detection for mobile satellite communication systems," IEEE Journal on Selected Areas in Communications, vol. 36, no. 2, pp. 280 - 291, Feb. 2018.
[33] C. Zhang, W. Cao, Z. Yang, K. Tian, and N. Zhang, "Random access preamble design for large frequency shift in satellite communication," Proc. 2019 IEEE 2nd 5G World Forum (5GWF), Sept. 2019.
[34] T. A. Khan and X. Lin, "Random access preamble design for 3GPP non-terrestrial networks," Proc. 2021 IEEE Globecom Workshops (GC Workshops), Dec. 2021.